Catal Lett (2007) 119:228–236
DOI 10.1007/s10562-007-9222-6

Hydrogen Production from Ethanol Steam Reforming Over Ni/CeO_2 Nanocomposite Catalysts

Humberto V. Fajardo · Luiz F. D. Probst · Neftalí L. V. Carreño · Irene T. S. Garcia · Antoninho Valentini

Received: 29 June 2007 / Accepted: 13 July 2007 / Published online: 4 August 2007

Abstract The organic polymer chitosan was used as the polymeric precursor for the synthesis of Ni/CeO_2 nanocomposite catalysts. The materials were characterized by N_2 physisorption, H_2 chemisorption, AA, XRD, TGA, TPR, SEM and TEM analyses. The catalysts provide very good reactivity in ethanol steam reforming compared to the conventional Ni/CeO_2 catalyst prepared by the impregnation method using a commercial support. High hydrogen selectivity (>75%) was obtained on Ni/CeO_2 catalysts by operating at a temperature range of 325–500 °C and a H_2O/C_2H_5OH molar ratio of 3. It was verified that the catalytic behavior could be influenced depending on the experimental conditions employed.

Keywords Hydrogen · Cerium oxide · Ethanol · Steam reforming

H. V. Fajardo (✉) · L. F. D. Probst
Departamento de Química- Pós-Graduação em Química, Universidade Federal de Santa Catarina, Centro de Ciências Físicas e Matemáticas, Campus Universitário, CP 476, Florianopolis, SC CEP 88040-900, Brazil
e-mail: hfajardo@qmc.ufsc.br; hfajardoufsc@hotmail.com

N. L. V. Carreño · I. T. S. Garcia
Departamento de Química Analítica e Inorgânica, Universidade Federal de Pelotas, Capao do Leao, RS CEP 96010-900, Brazil

A. Valentini
Departamento de Química Analítica e Físico-Química, Universidade Federal do Ceará, Fortaleza, CE CEP 60451-970, Brazil

1 Introduction

In recent decades, hydrogen production has attracted great interest because of the potential applications in fuel cells. A number of hydrogen generation routes have been proposed and explored including water electrolysis, gasification and pyrolysis processes, partial oxidation and steam reforming reactions. However, steam reforming is the most widely used process for hydrogen production from raw materials such as methanol, natural gas and gasoline, all of which are derived from fossil resources and their consumption releases greenhouse gases and local pollutants [1–6]. An alternative and promising way to produce hydrogen is to use ethanol as the feedstock for the steam reforming process. This alcohol has several advantages compared to fossil fuels but the most important is probably its renewable origin. It can be easily obtained from several biomass sources, including through the fermentation of sugarcane, becoming very interesting for Latin American countries with extensive plantations of this crop, especially Brazil, which leads the world in the production and use of ethanol from sugarcane for fuel. The bio-ethanol-to-hydrogen system has the positive feature of being CO_2 neutral, thus environmental friendly, since the CO_2 produced is consumed for biomass growth and a nearly closed carbon cycle results. In comparison to methanol, bio-ethanol is less toxic, making its handling, storage, transportation and distribution relatively safe and easy. In addition, bio-ethanol, which contains water in excess can be directly subjected to steam reforming, thereby eliminating the operation of distillation required to produce pure ethanol allowing the entire process be economically attractive [5–10].

The feasibility of hydrogen production from steam reforming of ethanol has been established theoretically [10–14]. Moreover, a number of publications report

experimental catalytic studies for the above-mentioned reaction, discussing the utilization of oxides (Al_2O_3, ZnO, La_2O_3, MgO) and noble- and non-noble metal-based catalysts (Ni/Al_2O_3, Rh/Al_2O_3, Ni/Al_2O_3–La_2O_3, Co/ZnO, Rh/CeO_2–ZrO_2). From the data reported, not only the operational conditions employed, but also the nature of the metal phase and support used, has been shown to influence the catalytic performance. Generally, acidic supports such as Al_2O_3 are known to favor the dehydration reaction to ethylene and water, followed by polymerization of ethylene to form coke. Obviously, the catalytic stability is affected since the carbon deposition promotes catalyst deactivation. On the other hand, basic supports such as MgO favor dehydrogenation to acetaldehyde and condensation reactions. The presence of these undesirable products, generated from these reactions, hinders the overall hydrogen production reducing the catalyst selectivity [7, 8]. Better catalytic performance, however, with good stability and high hydrogen selectivity can be expected over supports with redox properties, such as CeO_2 [15–18]. This oxide has been commonly used as a catalyst in a wide variety of reactions as well as an effective promoter for catalysts. This oxide has high oxygen mobility (redox properties) and a high oxygen storage capacity, and can act as a local source or sink for oxygen involved in reactions taking place on its surface. In addition, CeO_2 is known to enhance the reducibility and the dispersion of the supported metal. In spite of such interesting characteristics, the major limitation to applying CeO_2 as a support for metallic catalysts is its low specific surface area and poor textural stability under reduction conditions [17–23].

Therefore, the objective of the present study was to prepare a bifunctional catalyst based on nickel and cerium with relatively high specific surface area and efficiency for steam reforming of ethanol to produce hydrogen with high selectivity. The catalysts were prepared through a polymer-based precursor method using an intermediate hybrid polymer comprised of nickel, cerium, citric acid and the biopolymer chitosan. The activity toward ethanol steam reforming and the effect of reaction temperature and inlet steam content (water/ethanol molar ratio) were investigated, and compared to those of a conventional Ni/CeO_2 catalyst prepared by impregnation of a commercial support.

2 Experimental

2.1 Catalyst Synthesis

The nanocomposites were synthesized using nickel(II) nitrate ($Ni(NO_3)_2 \cdot 6H_2O$–Aldrich), citric acid (CA–Biotec) and cerium(III) nitrate ($Ce(NO_3)_3 \cdot 6H_2O$–Aldrich). Citric acid (0.20 mol) was dissolved in 250 mL of distilled water. The Ce and Ni nitrates were then added to the CA-aqueous solution and mixed for homogenization for 15 minutes at room temperature. A CA:metal ratio of 2:1 (in mol) was used. The metal concentration is the sum of Ce and Ni. The Ni/Ce ratio was 0.5 (in mol), which was later confirmed by atomic absorption measurements.

The chitosan solution, which was prepared by dissolving the chitosan powder (Aldrich) in distilled water containing acetic acid, was added to the citrate solution at a mass ratio of 20:60 in relation to the citric acid in order to promote the polymerization reaction. After polymerization at 100 °C for 3 h, the homogeneous solid resin was treated at 350 °C under air atmosphere. The resulting precursor compound was ground in a ball mill. The samples were then pyrolyzed for 1 h at two different temperatures, 500 °C (Ni/Ce#500) and 700 °C (Ni/Ce#700), under a N_2 flow rate of 1 mL/min. The conventional Ni/CeO_2 sample (Ni/Ce#c) was prepared by the impregnation of the CeO_2 support (Riedel-de Haën, Germany) with an aqueous solution containing the required amount of nickel nitrate hexahydrate. The water excess was removed by evaporation at 80 °C. This conventional sample was dried at 200 °C for 24 h and calcined in air at 650 °C for 2 h.

2.2 Catalyst Characterization

The crystal structure of the nanocomposites was characterized by X-ray diffraction (XRD) (Model D-5000, Siemens) using CuKα radiation and a graphite monochromator.

For the high-resolution transmission electron microscopy-HRTEM/TEM (200 kV Model CM200 Philips, Holland) study, a drop of the powder suspension was deposited on a carbon-covered Cu grid.

The sample morphology was observed on scanning electron micrographs (SEM), obtained with a Philips XL30 scanning electron microscope operating at an accelerating voltage of 20 kV.

The pyrolysis process was followed by thermogravimetric analysis (TGA) (model STA 409 Netzsch, Selb, Germany) using a 10 °C/min heating rate with a nitrogen or airflow of 20 mL/min.

Samples were characterized by N_2 adsorption/desorption isotherms obtained at the temperature of liquid nitrogen using an automated physisorption instrument (Autosorb-1C, Quantachrome Instruments). Specific surface areas were calculated according to the Brunauer–Emmett–Teller (BET) method, and the pore size distributions were obtained according to the Barret–Joyner–Halenda (BJH) method from the adsorption data.

Using the same equipment, the H_2 chemisorption of the catalysts was performed at 27 °C after activation of the sample in a flow of H_2 (30 mL/min) at 250 and 350 °C

(5 °C/min) for 1 h and evacuation for 1 h at the same temperature. The amount of irreversible H_2 uptake was obtained from the difference between the total adsorption of H_2 on the catalyst and a second adsorption series of H_2 determined after evacuation of the catalyst sample for 30 min at the same temperature (27 °C).

Temperature programmed reduction (TPR) analysis was performed in a quartz reactor under 5 vol% H_2/N_2 flow (30 mL/min) from 30 to 940 °C at a heating rate of 5 °C/min. A thermal conductivity detector (TCD) was used to monitor the H_2 consumption. A PM5A column trapped water formed during the process.

2.3 Catalytic Testing

Catalytic performance tests were conducted at atmospheric pressure with a quartz fixed-bed reactor (inner diameter 12 mm) fitted in a programmable oven, in the temperature range of 325–500 °C. The catalyst was previously reduced in situ under hydrogen atmosphere at 500 °C for 2 h. The water:ethanol mixture (molar ratios 1:3, 1:1 and 3:1) is pumped into a heated chamber and vaporized. The water-ethanol gas (N_2) stream (30 mL/min) is then fed to the reactor containing 100 mg of the catalyst. The reactants and the composition of the reactor effluent were analyzed with a gas chromatograph (Shimadzu GC 8A), equipped with a thermal conductivity detector (TCD), Porapak-Q and a 5A molecular sieve column with Ar as the carrier gas. Reaction data were recorded for 6 h. Catalyst activity was evaluated in terms of ethanol conversion. We defined ethanol conversion as (Eq. 1):

$$C_{EtOH}(\%) = (Q_{conv}/Q_{EtOH}) \times 100. \quad (1)$$

Here, Q_{conv} represents the quantity (moles) of converted ethanol; Q_{EtOH} represents the total quantity (moles) of ethanol feed into the reactor.

We defined the catalyst selectivity as the mole fraction of each product as (Eq. 2):

$$S_P(\%) = (Q_P/Q_{sP}) \times 100. \quad (2)$$

Here, Q_P represents the number of moles of each product; Q_{sP} represents the sum of the moles of the products, but the moles of solid products (such as small amount of coke) are not included.

3 Results and Discussion

Before the heat-treatment, thermogravimetric analyses were carried out in nitrogen atmosphere and air (Fig. 1). The difference in the weight elimination under N_2 and air atmospheres was significant. The two profiles presented the same behavior up to 300 °C. However, for temperatures higher than 300 °C the analysis carried out under airflow showed an expressive weight loss up to 500 °C, whereas the weight loss up to 500 °C for the analysis carried out under N_2 flow was less expressive. This result suggests the dependence of the residual organic elimination of the polymeric precursor on the annealing temperature and atmosphere. This observation reveals the possibility to obtain materials with different chemical properties by varying the heat treatment conditions. Based on the TG analysis, the pyrolysis of the samples was carried out in a two-step process. The first was to promote the organic structure cracking and also to partially eliminate the organic precursors. In this step, the polymeric precursor was heat-treated at 350 °C for 1 h under airflow. The second was carried out under N_2 atmosphere at 500 and 700 °C in order to promote a greater elimination of the residual material and the oxide phase formation.

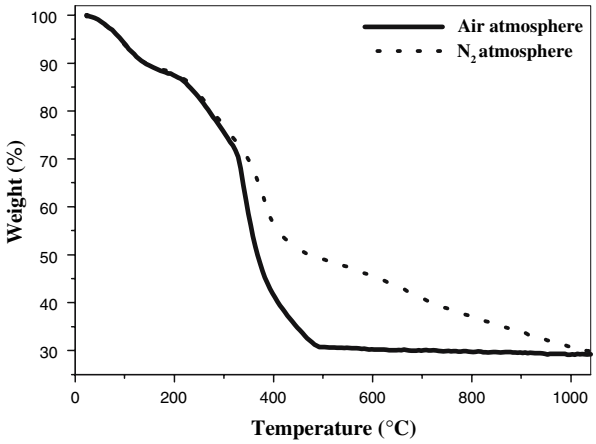

Fig. 1 Thermogravimetric analysis of the Ni/CeO_2 precursors, heating rate of 10 °C/min; sample mass of 10 mg; gas flow of 20 cm^3/min

It is known that CeO_2 commonly presents a low specific surface area and a low pore volume [19–20, 24]. Table 1 shows the specific surface area and pore volume of the Ni/CeO_2 samples heat-treated at different temperatures. As one can see, the heat-treatment has a great influence on the surface area and pore volume. A high temperature promotes a lower surface area. Even so, all the samples

Table 1 Specific surface area and pore volume of Ni/CeO_2 catalysts

Catalyst	S_{BET} (m^2/g)	V_{BJH} (cm^3/g)
Ni/Ce#500	51	0.037
Ni/Ce#700	36	0.028
Ni/Ce#c	5	0.004

S_{BET} = Specific surface area

V_{BJH} = pore volume

prepared by the hybrid polymer method presented better textural properties than the sample processed by the impregnation method. The nitrogen adsorption-desorption isotherm profiles of the Ni/Ce#500 and Ni/Ce#700 samples (not shown) revealed a non-porous or macroporous material, which is to be expected for Ni/CeO_2 samples. The changes in the textural properties observed for the Ni/CeO_2 nanocomposite samples, such as a decrease in the surface area and pore volume with an increase in the pore diameter, may be due to the residual carbon elimination as a consequence of the heat-treatment temperature increase. The presence of residual carbon may contribute to a high surface area.

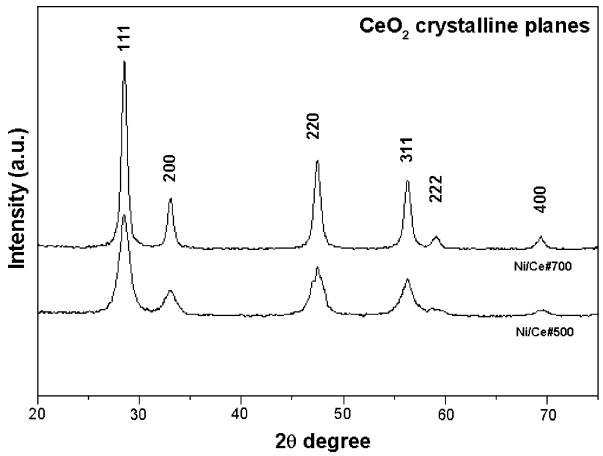

Fig. 2 XRD patterns of Ni/CeO_2 powders immediately after the annealing process at 500 and 700 °C for 1 h under a N_2 atmosphere

The results of the X-ray diffraction analysis carried out immediately after the annealing process are shown in Fig. 2. The sample heat-treated at a higher temperature presented a higher CeO_2 crystallinity, as is revealed by the X-ray peaks. All samples showed significant peaks at approximately 2θ values of 28.5, 33, 47.3 and 56.2°, which represent the indices of (111), (200), (220) and (311) planes of CeO_2, respectively. This shows the presence of a cubic fluorite structure in the Ni/CeO_2 catalysts prepared. However, the presence of the NiO phase was much less significant. This suggests that in Ni/CeO_2 catalysts, the NiO is highly dispersed as smaller NiO crystallites, which are not large enough for XRD detection. The XRD also revealed the absence of any other characteristic peak of a mixed oxide phase being formed due to an interaction between NiO and the CeO_2 support [21, 24–25].

The TPR profiles of the Ni/CeO_2 samples prepared (Fig. 3) show three major H_2 consumption peaks. The lower temperature peak is attributed to the reduction of free NiO particles, which aggregate on the surface of CeO_2 while the second peak is attributed to the reduction of strongly bound NiO on the support, being reduced to Ni^0 state. However, this second peak could also be attributed to

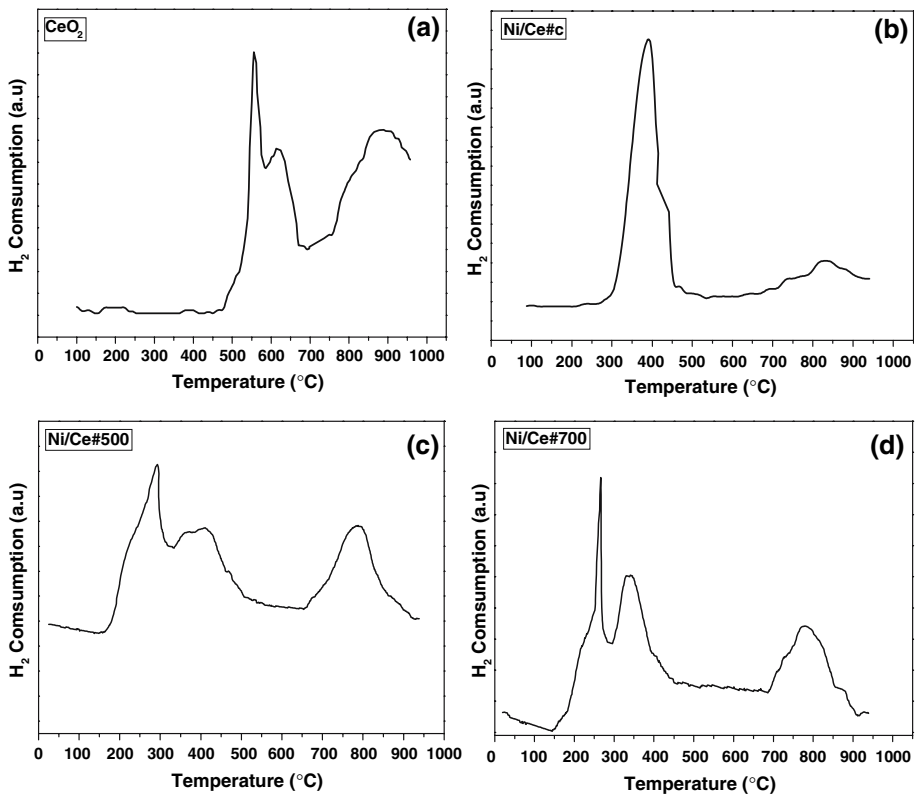

Fig. 3 Temperature programmed reduction (TPR) profiles of Ni/CeO_2 catalysts. (**a**) CeO_2; (**b**) Ni/Ce#c, (**c**) Ni/Ce#500 and (**d**) Ni/Ce#700

the partial reduction of the CeO_2 surface. Although there are no diffraction peaks of NiO in the XRD patterns, the aggregated NiO particles may be present as small particles or in amorphous phase, which could be reduced into metallic nickel together with the reduction of surface ceria. The higher temperature broad peak is assigned to the reduction of bulk CeO_2 [21–22, 24–26]. It is important to point out that the TPR profile of the pure commercial CeO_2 also showed three H_2 consumption peaks. The reduction of CeO_2 started around 450 °C and three reduction peaks appeared at around 550, 620 and 890 °C, respectively. This is in agreement with results reported in the literature where three peaks with closer reduction temperatures were observed for pure ceria [27]. According to Shyu et al. [27], the reduction of ceria capping oxygen would be occur at around 593–753 K, forming a non-stoichiometric species at 755 K and the reduction of bulk CeO_2 from Ce^{4+} to Ce^{3+} would occur at 1073 K. However, all of them at higher temperatures than those of the Ni/CeO_2 samples. This can be explained by the presence of Ni on the CeO_2 surface, which acts as a catalyst in the CeO_2 reduction leading to a shift of the H_2 consumption peaks to lower temperatures. The TPR profile of the Ni/CeO_2 sample prepared by the impregnation method shows that the major H_2 consumption peak in the range between 300 and 500 °C is due to the NiO reduction.

With the aim of obtaining more information on the surface properties of the Ni/CeO_2 catalysts prepared, H_2 adsorption was carried out. H_2 chemisorption is recommended to determine the metal dispersion. The occurrence of significant H_2 chemisorption on CeO_2, which may mask the results of the determination of the metal surface area [28], should be considered. Nevertheless, H_2 chemisorption results can help in the interpretation of the reduction process of the catalysts. The results for total and irreversible H_2 chemisorption summarized in Table 2, suggest an increase in the metal surface area for all the samples with increasing activation temperature. The sample calcined at 500 °C showed a higher H_2 chemisorption. This suggests that the metal surface is more accessible to the H_2 adsorption in this sample. On the other hand, the sample calcined at 700 °C shows a low metal surface area, indicating a sintering process, which is in agreement with its lower specific surface area.

Figure 4a shows a bright field (BF) transmission electron microscopy (TEM) image of the Ni/Ce#500 sample, showing Ni nanoparticles (dark spots on the photograph) embedded and dispersed within the CeO_2 matrix and

Table 2 Metal surface area determined by H_2 chemisorption

		Ni/Ce#500		Ni/Ce#700	
H_2 (m^2/g)		250	350	250	350
	Total	11.4	14.1	4.9	9.9
	Irreversible	7.8	8.1	2.4	3.8

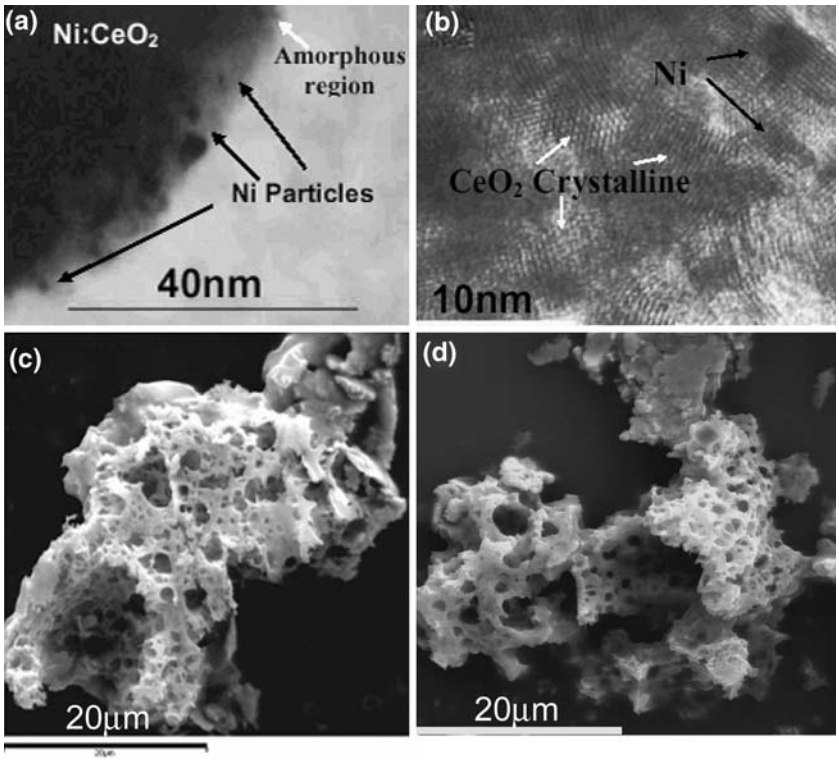

Fig. 4 BF-TEM image (**a**) and HR-TEM image (**b**) of the Ni/CeO_2 nanocomposite catalyst heat-treated at 500 °C. SEM images: (**c**) Ni/CeO_2 nanocomposite catalyst heat-treated at 500 °C and (**d**) Ni/CeO_2 nanocomposite catalyst heat-treated at 700 °C

amorphous carbon. The high-resolution transmission electron microscopy (HRTEM) image (Fig. 4b) reveals that the Ni particles (illustrated by black arrows) distributed within the nanocrystalline ceria matrix (illustrated by white arrows) have an average particle size of 4 nm. The pore diameters shown in the SEM images given in Fig. 4c and d are quite different to those determined from the N_2 adsorption isotherm. Nevertheless, these images do illustrate the particular morphology of the Ni/CeO_2 samples. The Ni/Ce#500 and Ni/Ce#700 samples have a spongy appearance, which is the result of the carbon elimination during the annealing process. During the precursor elimination by decomposition, the gas generated opens channels through the oxide matrix, which results in a sample with spongy appearance.

In order to investigate the catalytic activity of the Ni/CeO_2 samples, the steam reforming of ethanol was carried out. The influence of operating temperature and inlet H_2O/C_2H_5OH molar ratio on the ethanol conversion and product selectivities from the ethanol steam reforming over Ni/CeO_2 catalysts was studied by varying the temperature from 325 to 500 °C and the inlet H_2O/C_2H_5OH molar ratio from 3 to 1/3. The catalytic behaviors of the different Ni/CeO_2 samples (Ni/Ce#500, Ni/Ce#700 and Ni/Ce#c) were also studied and compared.

The reaction pathway during catalytic ethanol steam reforming comprises a series of simultaneous reactions, including decomposition, dehydrogenation, dehydration and steam reforming reactions. These reactions are more or less promoted depending on the nature of the catalyst, the type of interaction with the surface of the solid material and the different reaction conditions [6–8]. Typical experimental results obtained are presented in Fig. 5, in which the selectivity of each product and the conversion of ethanol are shown as a function of reaction temperature. As expected, the conversion of ethanol increased with increasing reaction temperature. The complete conversion of ethanol was achieved when the temperature was 400 °C and above. From the results of Fig. 5, it can be seen that H_2, CO_2, CO, CH_4 and CH_3CHO were the only products detected during the ethanol steam reforming process in the range of reaction temperatures studied. At 325 °C, the conversion of ethanol reached 27.5% at the beginning of the test. However, the ethanol conversion decreased from 27.5% to 1% after 300 min in time on stream with very little difference in the product distribution. The process at this temperature was highly selective to hydrogen production and CH_3CHO was the major by-product, with lower amounts of CH_4. It is observed that the steam reforming reaction of ethanol (Eq. 3) is negligible.

$$C_2H_5OH + 3H_2O \rightarrow 2CO_2 + 6H_2 \quad (3)$$

Instead, ethanol dehydrogenation to acetaldehyde (Eq. 4) and an ethanol decomposition reaction (Eq. 5) seem to occur as the main reactions.

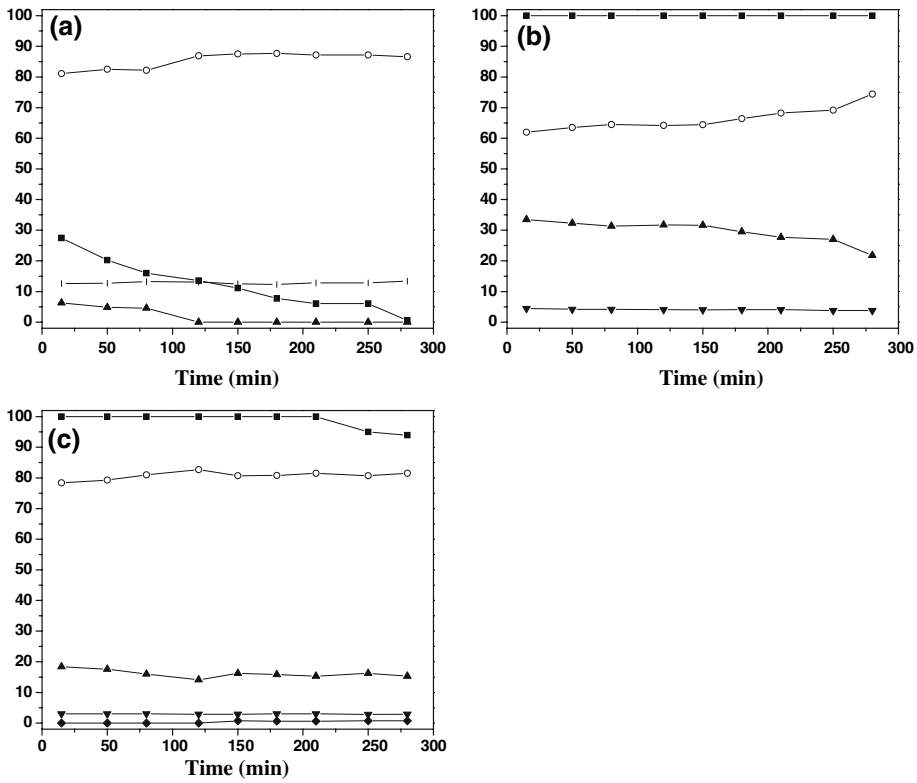

Fig. 5 Effect of reaction temperature on catalytic performance in the steam reforming of ethanol over Ni/Ce#500 catalyst with a H_2O/C_2H_5OH molar ratio = 3. (**a**) 325 °C, (**b**) 400 °C and (**c**) 500 °C. Legends: ■ = C_2H_5OH conversion; o = H_2; l = CH_3CHO; ▲ = CH_4; ▼ = CO_2; • = CO selectivity, respectively

$$C_2H_5OH \rightarrow CH_3CHO + H_2 \quad (4)$$

$$C_2H_5OH \rightarrow 2H_2 + 2C + H_2O \quad (5)$$

During the last 200 min the formation of CH_4 decreased as the concentration of H_2 increased and the CH_3CHO formation remained constant. This suggests that the decomposition of CH_4 to H_2 and C (Eq. 6) takes place.

$$CH_4 \rightarrow 2H_2 + C \quad (6)$$

The coke formation from decomposition reactions of methane and ethanol may be considered as the main reason for the catalyst deactivation observed in this case. When the temperature increased to 400 °C the conversion of ethanol reached 100%, remaining stable until the end of the run. The main carbon compounds obtained at this temperature were methane and carbon dioxide. The difference between the formation of CO_2 and H_2 may be due to the great quantities of coke deposited on the catalyst. However, it should be highlighted that this deposition did not affect the activity of the catalyst Ni/Ce#500 during the reaction period. A decrease in the selectivity of hydrogen was observed, while the selectivity of methane increased and no acetaldehyde was detected. This indicates that at this stage the ethanol decomposition reaction (Eq. 7) and the water gas shift reaction (Eq. 8) were the main reactions involved.

$$C_2H_5OH \rightarrow H_2 + CH_4 + CO \quad (7)$$

$$CO + H_2O \rightarrow CO_2 + H_2 \quad (8)$$

Apparently, the CO produced by ethanol decomposition was subsequently converted into CO_2 and H_2 through the water gas shift reaction and/or possibly through CO oxidation promoted by CeO_2 (Eq. 9).

$$2CO + O_2 \rightarrow 2CO_2 \quad (9)$$

It is known that Ni/CeO_2 catalysts efficiently convert CO to CO_2 via the water gas shift reaction and CeO_2 can promote hydrocarbon oxidation due to its redox properties [18, 29–30]. The Boudouard reaction (Eq. 10) may be adding to the amount of CO_2 observed at this temperature, while methanation reactions (Eq. 11 and Eq. 12) could be contributing to the observed CH_4 concentration.

$$2CO \rightarrow C + CO_2 \quad (10)$$

$$CO + 3H_2 \rightarrow CH_4 + H_2O \quad (11)$$

$$CO_2 + 4H_2 \rightarrow CH_4 + 2H_2O \quad (12)$$

The selectivity for H_2 began to increase at the end of the run suggesting that the catalytic decomposition of methane is most likely responsible, since the CO_2 concentration remained stable. At the highest reaction temperature, the selectivity toward CH_4 decreases, H_2 selectivity increased, CO_2 selectivity remained relatively constant and CO concentration passed through a maximum. This behavior may be due to both the reaction of methane steam reforming (Eq. 13) and the reverse water gas shift reaction (Eq. 14) which are favored at elevated temperatures [7–8, 31].

$$CH_4 + H_2O \rightarrow CO + 3H_2 \quad (13)$$

$$CO_2 + H_2 \rightarrow CO + H_2O \quad (14)$$

Figure 6 shows the effect of the H_2O/C_2H_5OH molar ratio on the reforming performance at 400 °C. It can be observed that H_2O/C_2H_5OH molar ratio plays an important role in ethanol conversion. It was indicated that by increasing the H_2O/C_2H_5OH molar ratio the ethanol conversion is favored. In addition, a significant effect upon decreasing the water content was to decrease the catalyst stability. This fact was to be expected due to carbon deposition, which is favored for lower H_2O/C_2H_5OH molar ratio values. It is well established that deactivation of supported metal catalysts during ethanol steam reforming occurs mainly due to carbon deposition [7–14]. It is interesting to note that whatever the amount of water initially introduced, the selectivity values of the main products remain almost constant. However, the concentration of CO in the outlet gas stream increased with the decreased in the water to ethanol ratio, probably due to the reverse water gas shift reaction, which is driven by the low water concentration.

Figure 7 illustrates the ethanol conversion and product distributions in ethanol steam reforming at 400 °C over the different Ni/CeO_2 catalysts. The catalysts heat-treated at 500 and 700 °C showed similar activity behavior and product selectivity. The higher calcination temperature caused the sintering of the material resulting in a reduction in its specific surface area, from 51 to 36 m^2/g. This caused greater changes in the catalytic activity of Ni/Ce#700, however, changes in the activity of the catalyst calcinated at 500 °C were not observed, due to the complete conversion during the reaction period. The high initial reforming activity and further deactivation observed for Ni/Ce#700 catalyst suggest that some of the nickel atoms have an enhanced activity in spite of the lower metal dispersion. However, the Ni/Ce#500 catalyst was more active than the Ni/Ce#700 catalyst, the former achieving the complete conversion of ethanol and remaining stable until the end of the test. This may be related to the more effective action of the active phase, which covers a greater area (higher metal surface dispersion) in this sample. In the presence of nickel the catalyst becomes more active and the

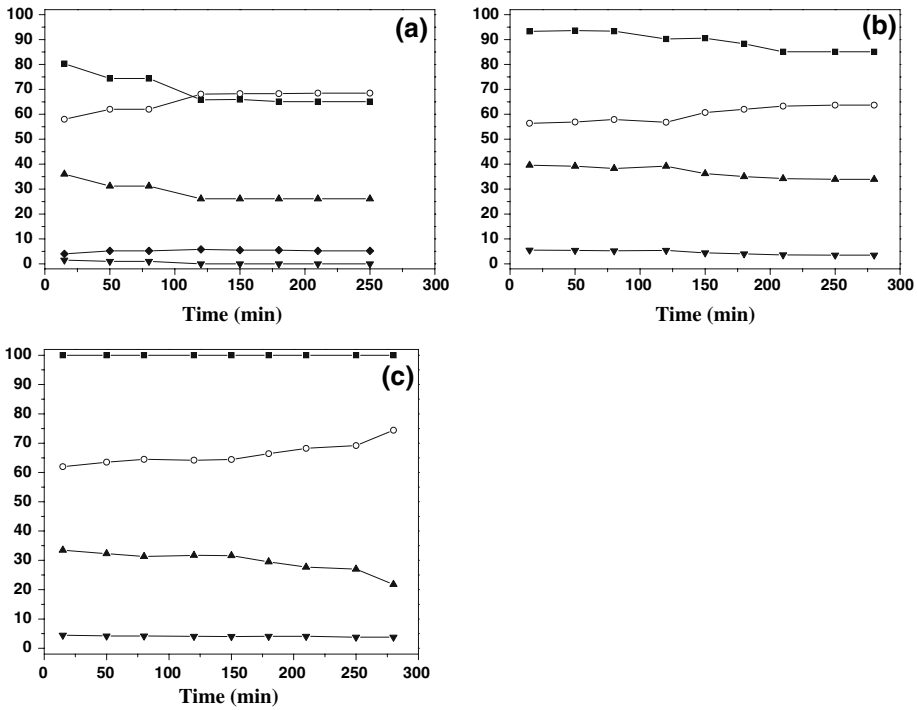

Fig. 6 Effect of H_2O/C_2H_5OH molar ratio on catalytic performance in the steam reforming of ethanol over Ni/Ce#500 catalyst at 400 °C. (**a**) 1/3, (**b**) 1/1 and (**c**) 3/1. Legends: ■ = C_2H_5OH conversion; o = H_2; ▲ = CH_4; ▼ = CO_2; • = CO selectivity, respectively

active metal site may be responsible for the breaking of the C–C and C–H bonds in the ethanol cleavage to produce H_2, CH_4 and CO_2 [31, 32]. On the other hand, ethanol conversion was the lowest with the Ni/Ce#c catalyst. This is probably due to the low specific surface area of this sample. It is interesting to observe that ethylene and acetaldehyde were the only by-products formed during ethanol steam reforming over Ni/Ce#c. Moreover, this particular catalyst was unique in that ethylene was observed in the product stream. It is well known that physicochemical properties of a catalyst play an important role in the evolution of surface reactions. In ethanol steam reforming both dehydrogenation to acetaldehyde or dehydration to ethylene (Eq. 15) can occur depending upon the nature of the catalyst [7, 8].

$$C_2H_5OH \rightarrow C_2H_4 + H_2O \quad (15)$$

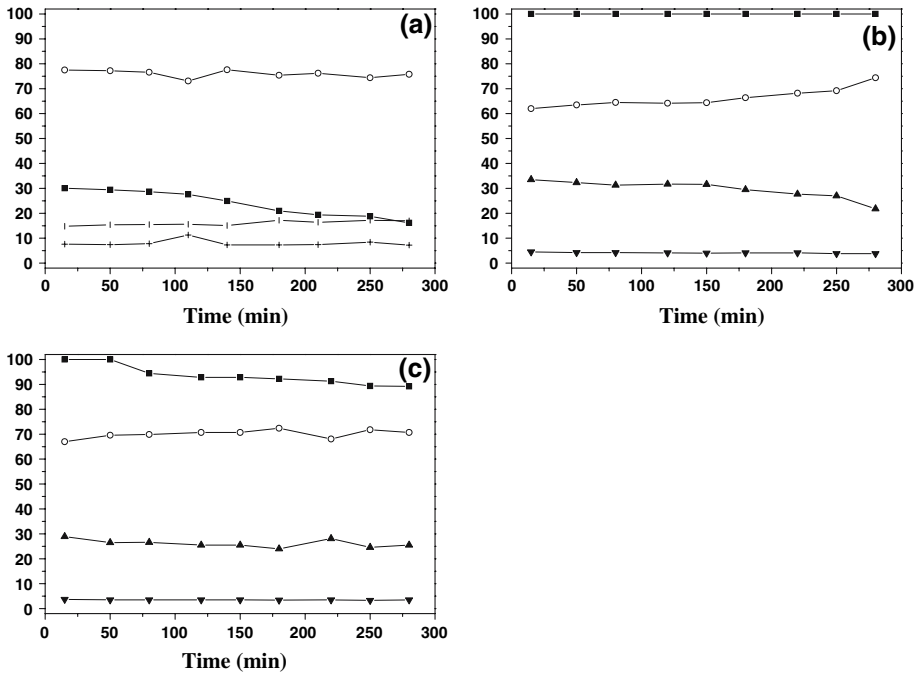

Fig. 7 Catalytic performance in the steam reforming of ethanol of the different Ni/CeO_2 samples at 400 °C with a H_2O/C_2H_5OH molar ratio = 3. (**a**) Ni/Ce#c, (**b**) Ni/Ce#500 and (**c**) Ni/Ce#700. Legends: ■ = C_2H_5OH conversion; o = H_2; l = CH_3CHO; ▲ = CH_4; ▼ = CO_2; + = C_2H_4 selectivity, respectively

Dehydration and dehydrogenation reactions are promoted over the Ni/Ce#c catalyst surface. Thus, a combination of catalytic properties is observed. Although Ni/Ce#c also provides high selectivity toward H_2 production, the major weaknesses of this catalyst is its low specific surface area resulting in low redox properties. Consequently, the lowest ethanol steam reforming reactivity was observed over this catalyst. Literature studies indicate that the enhancement of the redox properties of CeO_2 leads to an improvement in the reforming activity of cerium oxide-based catalysts [19, 20]. The absence of ethylene in the effluents of Ni/Ce#500 and Ni/Ce#700 catalysts is an indication of very low ethanol dehydration rates. Furthermore, in the literature it is reported that CeO_2 is a moderate catalyst for the dehydration reaction, confirming the high reforming activity presented by these catalysts.

4 Conclusion

In this study, a promising method of obtaining Ni/CeO_2 catalysts was presented. It was observed that the methodology used in the preparation led to the obtainment of materials with important properties for applications in catalytic processes, such as ethanol steam reforming. The catalysts prepared in this study showed high specific surface area and pore volume compared to a Ni/CeO_2 catalyst prepared by impregnation method of a commercial support. The results clarify that the Ni/CeO_2 catalysts produced a hydrogen-rich gas mixture and have high activity for ethanol steam reforming. It was observed that the reaction conditions and the nature of the Ni/CeO_2 samples influenced the ethanol steam reforming process. The Ni/Ce#500 catalyst exhibited the highest activity and stability during the ethanol steam reforming process. It was also found that it was very selective toward hydrogen production at a reaction temperature of 400 °C and with a H_2O/C_2H_5OH molar ration of 3. Based on the results obtained, acetaldehyde seems to be a intermediate product formed, which may be further decomposed producing H_2, CH_4 and carbon oxides. Moreover, it is interesting to note that the concentration of CO was very low in the effluent compositions.

Acknowledgments The authors gratefully acknowledge CNPq and FINEP for financial support.

References

1. Armor JN (2005) Catal Lett 101:131
2. Brown LF (2001) Int J Hydrogen Energy 26:381
3. Joensen F, Rostrup-Nielsen JR (2002) J Power Sources 105:195
4. Rostrup-Nielsen JR, Rostrup-Nielsen T (2002) CATTECH 6:150
5. Demibras A (2007) Progress Energy Combus Sci 33:1
6. Idriss H (2004) Platinum Metals Rev 48:105
7. Vaidya PD, Rodrigues AE (2006) Chem Eng J 117:39
8. Haryanto A, Fernando S, Murali N, Adhikari S (2005) Energy & Fuels 19:2098
9. Manzini F (2006) Int J Hydrogen Energy 31:327
10. Garcia EY, Laborde MA (1991) Int J Hydrogen Energy 16:307
11. Cavallaro S, Freni S (1996) Int J Hydrogen Energy 21:465
12. Vasudeva K, Mitra N, Umasankar P, Dhingra SC (1996) Int J Hydrogen Energy 21:13
13. Fishtik I, Alexander A, Datta R, Geana D (2000) Int J Hydrogen Energy 25:31
14. Mas V, Kipreos R, Amadeo N, Laborde M (2006) Int J Hydrogen Energy 31:21
15. Zhang B, Tang X, Li Y, Cai W, Xu Y, Shen W (2006) Catal Commun 7:367
16. Nishiguchi T, Matsumoto T, Kanai H, Utani K, Matsumura Y, Shen WJ, Imamura S (2005) Appl Catal A 279:273
17. Roh HS, Wang Y, King DL, Platon A, Chin YH (2006) Catal Lett 108:15
18. Kugai J, Velu S, Song C (2005) Catal Lett 101:255
19. Laosiripojana N, Sutthisripok W, Assabumrungrat S (2007) Chem Eng J 127:31
20. Laosiripojana N, Assabumrungrat S (2006) Appl Catal B: Environ 66:29
21. Chary KVR, Rao PVR, Vishwanathan V (2006) Catal Commun 7:974
22. Li Y, Zhang B, Tang X, Xu Y, Shen W (2006) Catal Commun 7:380
23. Valentini A, Probst LFD, Carreño NLV, Leite ER, Pontes FM, Longo E, Schreiner WH, Lisboa-Filho PN (2003) Quim Nova 26:648
24. Valentini A, Carreño NLV, Probst LFD, Barison A, Ferreira AG, Leite ER, Longo E (2006) Appl Catal A 310:174
25. Xu S, Yan X, Wang X (2006) Fuel 85:2243
26. Fajardie F, Tempere JF, Manoli JM, Djega-Mariadassou G (1998) J Chem Soc Faraday Trans 94:3727
27. Shyu JZ, Weber WH, Gandhi HS (1988) J Phys Chem 92:4964
28. Bernal S, Calvino JJ, Cauqui MA, Gatica JM, Cartes CL, Omil JAP, Pintado JM (2003) Catal Today 77:385
29. Yee A, Morrison SJ, Idriss H (2000) J Catal 191:30
30. Sheng PY, Bowmaker GA, Idriss H (2004) Appl Catal A 261:171
31. Fatsikostas AN, Verykios XE (2004) J Catal 225:439
32. Fajardo HV, Probst LFD (2006) Appl Catal A 306:134